Journal of Physics D: Applied Physics

PAPER

Surface-phonon-polariton-mediated photon response of terahertz quantum-well infrared photodetectors

To cite this article: DiXiang Shao *et al* 2019 *J. Phys. D: Appl. Phys.* **52** 035105

IOP Publishing Journal of Physics D: Applied Physics
J. Phys. D: Appl. Phys. **52** (2019) 035105 (6pp) https://doi.org/10.1088/1361-6463/aaeb77

Surface-phonon-polariton-mediated photon response of terahertz quantum-well infrared photodetectors

DiXiang Shao[1], XuGuang Guo[1], YiMing Zhu[1], SongLin Zhuang[1], ZhangLong Fu[2] and JunCheng Cao[2]

[1] Shanghai Key Lab of Modern Optical Systems, Terahertz Technology Innovation Research Institute, and Engineering Research Center of Optical Instrument and System, Ministry of Education, University of Shnaghai for Science and Technology, 516 Jungong Road, Shanghai 200093, People's Republic of China
[2] Key Laboratory of Terahertz Solid-State Technology, Shanghai Institute of Microsystem and Information Technology, Chinese Academy of Sciences, 865 Changning Road, Shanghai 200050, People's Republic of China

E-mail: xgguo_sh@qq.com and jccao@mail.sim.ac.cn

Received 17 July 2018, revised 21 October 2018
Accepted for publication 25 October 2018
Published 14 November 2018

Abstract

A surface-phonon-polariton (SPHP)-mediated photon response near the longitudinal optical (LO) phonon frequency of GaAs is investigated in a terahertz GaAs/AlGaAs quantum-well infrared photodetector, integrated with a one-dimensional metal grating. For a contrast device without a grating coupler, no SPHP-related signature is found in the photocurrent spectrum, because the incident radiation from free space cannot excite the SPHP, due to the mismatch of momentum. The intensity of the electric field component along the growth direction of the device absorption layer is numerically calculated. The results show that the photocurrent response peaks near the LO phonon frequency band (8.8–9.0 THz) are attributed to the local field enhancement induced by SPHP. Our results are useful to realize high performance SPHP-mediated terahertz photodetectors and other related terahertz devices.

Keywords: terahertz, quantum detectors, surface plasmon polaritons

(Some figures may appear in colour only in the online journal)

1. Introduction

Terahertz detectors are key components for both active and passive terahertz application systems [1–3]. There are various well-developed terahertz detectors [4]; for example, zero-bias photoconductive antennas based on optical rectification and heterodyne mixing processes [5], terahertz-field rectification detectors (field-effect transistors made by semiconductors and graphene), thermal terahertz detectors (made of Si, VO_x, $LaTiO_3$, and other thermo-electrical materials) [1, 4], and terahertz photodetectors (based on inter-subband transitions in low-dimensional semiconductor structures and impurity band to conduction/valence band transitions in extrinsic semiconductors) [4, 6, 7]. For terahertz detectors, high absorption efficiency is prompted to improve signal and suppress noise. However, due to the long wavelength of terahertz radiation and the diffraction limit, the terahertz radiation energy cannot be effectively focused onto the detectors by using traditional optical lenses [6, 8–10]. For terahertz photodetectors, the problem of low absorption efficiency becomes even worse. In such detectors, since the energy difference between the ground states and the excited states is very small (several meV to ~10 meV, determined by the energy of terahertz photons), to suppress the thermalized dark current, the doped concentration of electron/hole in ground states must be very small (~10^{16}–10^{17} cm^{-3}) [6]. To improve the absorption efficiency, various light couplers and concentrators have been developed for photodetectors working in the infrared and terahertz bands [11–18].

Terahertz quantum-well infrared photodetectors (QWIPs) are photoconductive-type detectors [6, 8, 9]. A terahertz

QWIP is composed of top and bottom metal electrodes, two doped semiconductor contact layers, and a multi-quantum-well (MQW) absorption layer with carriers doped in each QW between the two contact layers. In the dark state, because carriers confined in the QWs cannot directly tunnel across the thick barrier between two QWs, the current across a biased terahertz QWIP originates from the thermalized carriers, which is very small at low temperatures (<20 K for terahertz QWIPs). However, when the terahertz QWIP is illuminated with terahertz radiation whose energy matches the energy difference between the ground subband and the excited subbands, carriers confined in the QWs can absorb the terahertz photons and make a transition to the excited subands and the continuum states. These carriers in excited states will move across the terahertz QWIP to form a photocurrent under the biased electric field. Terahertz QWIPs have many advantages, such as high responsivity (~1 A W^{-1}) and normalized detectivity (~10^{10} Jones) [19], fast response (sub-nanosecond time scale) [20, 21], and designable peak response frequencies in a wide frequency range (3.0–30.0 THz) [6, 10]. However, terahertz QWIPs have some shortcomings that limit the further improvement of device performance. First, due to the lower barrier height and small energy difference between ground subband and excited subbands, the barriers should be thick enough to prohibit direct carrier tunneling. The carrier doping concentration in QWs must be low enough to suppress thermalized dark current, both of which lead to a very small effective absorption coefficient. For a device thickness of ~3.5 μm, the value of quantum absorption efficiency is in the range of 1%–5% [6, 8, 9]. Second, the polarization selection rule of inter-subband transition determines that only the field component parallel to the growth direction of MQWs can lead to the inter-band transition from ground subband to excited states [6].

In order to overcome the above-mentioned shortcomings of QWIP, various light couplers have been proposed and fabricated to increase the absorption efficiency [13, 17–19]. Diffractive gratings have been used as optical couplers of QWIPs working in the infrared regime to change the propagation direction of transverse magnetic (TM) light normally impinging on devices, in other words, to obtain the field component along the growth direction of QWs [6]. In the terahertz regime, metal grating couplers have been used not only to diffract terahertz beams, but also to obtain an enhanced local field near the edges of metal strips corresponding to the high order evanescent diffraction modes [17–19, 22]. The evanescent field can effectively extend to the MQW region due to the long wavelength of the terahertz wave and thin MQW absorption layer. In recent years, micro-cavities and photonic crystal slabs were introduced to enhance the absorption efficiency of QWIPs [13–16]. In such devices, the MQW absorption layers are inserted into these periodic-sub-wavelength cavities. Due to the excitation of resonant guided modes, the terahertz field can be effectively squeezed into the micro-cavity at resonant frequencies, and the interaction between the resonant guided modes and the confined carriers in QWs is strongly enhanced. Terahertz surface plasmon polaritons (SPPs) supported by an air-doped-semiconductor interface [23] have also been proposed to increase the absorption efficiency of terahertz QWIPs [12, 18]. However, due to the strong carrier-carrier scattering, the propagation of SPPs is always accompanied by severe Joule loss, weakening the effect of local field enhancement [23].

Surface phonon polaritons (SPHPs) are another type of low-energy excitations supported by semiconductor surfaces [24]. SPHPs in SiC, SiO_2, GaP, and two-dimensional (2D) van der Waals hetero-structures have been intensively investigated in relation to problems of strong light–matter interactions, sub-wavelength focusing, surface Raman enhancement spectroscopy, and controllable coherent thermal emitters [24–33]. In comparison with SPPs, in high quality crystals, due to the much weaker optical phonon–phonon scattering, the collective excitations of SPHPs have longer coherence time and smaller loss, which are favored to obtain SPHP-induced strong local field enhancement.

In this work, the feature of SPHP-mediated photoresponse near the longitudinal optical (LO) phonon frequency of GaAs is observed in a terahertz QWIP integrated with one-dimensional (1D) metal grating (G-QWIP). For a device without a grating coupler, no SPHP-related signature is found in the photocurrent spectrum, because the incident radiation from free space cannot excite the SPHPs due to the mismatch of momentum. We compute the volume-integrated square of electric field (VISE) component along the growth direction of QWs in the MQW layer with respect to frequency. It is found that the photocurrent feature near the LO phonon frequency band (8.8–9.0 THz) contributes to the local field enhancement. By fitting the computed VISE spectrum with the experimental photocurrent spectrum, the scattering rate of transverse optical (TO) phonon is derived, which is much smaller than that of SPPs. However, the two resonant frequencies (8.84 THz and 8.98 THz) cannot be determined through the dispersion relation of SPHP supported in vacuum-GaAs interface and the in-plane wave-vector provided by the grating because of the influences of surrounding metal strips and doped contact layers. Numerical calculations show that the doping concentration of up- and bottom-contact layers has remarkable effects on the behavior of SPHP. Our results are useful to realize SPHP-mediated terahertz photodetectors and other related terahertz devices.

2. Device design, fabrication, and characteristics

The GaAs/AlGaAs 2D structures are used to fabricate the terahertz QWIPs due to the mature material growth technique, good crystal and interface quality, and appropriate band offset. The device structure is grown by molecular beam epitaxy (MBE) on a semi-insulating GaAs substrate of 650 μm thick. The MBE layers consist of three parts (starting from the substrate). First, an 800 nm GaAs bottom contact layer doped with Si to 2×10^{17} cm^{-3} is grown on the substrate. Next are 40 periods of 12 nm wide GaAs wells and 60 nm thick AlGaAs barriers with Al mole fraction of 7.1%. In the central 10 nm region of each GaAs well, the concentration of Si dopant is 1×10^{17} cm^{-3}. Finally, a 400 nm GaAs layer doped with Si to

2×10^{17} cm^{-3} is grown as a top contact layer. The composition and period of MQWs are confirmed by x-ray diffraction and scanning electron microscopy. Only a slight difference is observed from the designed parameters. A conventional planar semiconductor fabrication process is carried out to realize the terahertz QWIPs. Square mesas of 1.0×1.0 mm^2 are formed by wet etching with an etch solution of H_3PO_4 (1):H_2O_2 (1):H_2O (25). The top and bottom metallic contacts of Ge/Au/Ni/Au with 40/80/35/300 nm are deposited by electron-beam evaporation and annealed at 370 °C for 30 s. In order to study the effects of SPHP, devices with and without a 1D metal grating coupler are fabricated, with the other device parameter being the same. The period of 1D grating is 15 μm with 50% duty cycle. The grating strips are composed of Ti/Pt/Au of 25/55/200 nm thick that are evaporated and lift-off inside the ring top contact.

The band structure of the terahertz QWIP is numerically calculated by solving the coupled Schrödinger and Poisson equations self-consistently, and the many-body effects are considered under the local density approximation [34]. Figure 1 shows the band structure and density of states (DOS) of the QWIP at zero bias and at temperature of 5.0 K. The growth direction of QWs is chosen to be the z axis. The peak response frequency corresponding to the gap between the ground state to the first excited subband, which is about 9.9 THz. The designed peak response frequency is about 0.9 THz higher than the LO frequency. Such a difference will decrease the transition strength at the LO frequency, but has no essential effects on the main results of this work. Moreover, there exists large spectral broadening due to the finite lifetime of electrons in excited states and the variations of well width and barrier height. (The starting point of photocurrent spectrum is at about 6.0 THz, see figure 2 below.) The DOS curve shows that the first and second subbands are localized states, and other higher states are quasi continuum above the barrier. The first excited subband is about 10 meV below the top of the barrier. This will guarantee a large value of transition strength. Meanwhile, a larger bias can be applied to the device to shorten the transit time of photon-excited electrons and increase the responsivity of the device.

Figure 2 shows the photocurrent spectra of the G-QWIP and the device without grating (C-QWIP). The spectral data are measured with a Fourier transform infrared spectrometer (Bruker VERTEX 80V). The frequency resolution is set to 0.1 cm^{-1}, and the sample chamber is evacuated to avoid water vapor absorption of terahertz radiation. For the G-QWIP, terahertz wave impinges on the device at the surface normal. In order to obtain the field component along the growth direction of QW, the C-QWIP is illuminated obliquely at an incident angle of 15 degrees. The broadband response spectra begin at about 6.0 THz. The response gap between 8.00–8.75 THz is due to the *reststahlen* band of GaAs [35]. The sawtooth structure in the range of 6.5–7.5 THz is attributed to the Fabry–Pérot interference of the dielectric cavity composed of the MBE-growth MQW layer and the substrate [22]. At frequencies above 7.5 THz, because of the absorption of optical phonons, the terahertz wave in the device cannot finish a roundtrip between the two interfaces of the cavity and no such sawtooth structure exists. For both devices, except the second-order diffractive satellite peak at 7.7 THz (G-QWIP), the shapes of the response spectra from 6.5 THz to 8.0 THz are nearly the same because the first-order diffraction channel opens at lower frequency of about 5.5 THz with the grating period of 15 μm. There is a great difference at about 9.0 THz between the two devices. For the C-QWIP, there is only a response peak (8.94 THz) that is introduced by the polarization field of LO phonon [36, 37]. However, for the G-QWIP, there are two response peaks at 8.84 THz and 8.98 THz. We attribute the two peaks to the SPHP-induced local field enhancement (detailed discussions shown below). For the C-QWIP, there is no measurable photocurrent signal when the incident terahertz radiation propagates along the surface normal direction, which is in agreement with [38]. Therefore, it indicates that the light scattering from the metal ring contact and other dielectric discontinuities has no effects on the photocurrent response.

Figure 3 depicts the dark current and peak responsivity with respect to the bias of the terahertz G-QWIP at a working temperature of 5.0 K. The dark current–voltage (I–V) curve is symmetric in the bias voltage (V) ranges of $1.0\,\mathrm{V} < |V| < 2.0\,\mathrm{V}$ and $|V| < 0.7$ V. In the region of $0.7\,\mathrm{V} < |V| < 1.0$ V, the current jumps rapidly and there exists a slight asymmetry between the negative and positive biases. The current sharp jump is due to the negative differential resistance (NDR) phenomenon in the current-sweeping mode [39]. The NDR will introduce a hysteresis in the voltage-sweeping mode, which is responsible for the asymmetry of the I–V curve in the $0.7\,\mathrm{V} < |V| < 1.0\,\mathrm{V}$ region. Therefore, we conclude that the electron transport across the device under negative and positive biases shows the same behavior. The blackbody responsivities at different biases are measured with a calibrated blackbody (cavity blackbody IR-564/301) at temperature of 1000 K, and the peak responsivities (8.98 THz) are derived from the photocurrent spectrum. The peak responsivity at positive bias is larger than that at the corresponding negative bias with the same absolute value. The bias-polarization-dependent responsivity may be due to the position deviation of Si doping from the central region of QW [6].

3. Numerical results and discussions

We define a quantity γ, the field component along the growth direction z of QW of VISE, to describe the effect of the grating on the photoresponse of the G-QWIP,

$$\gamma(\omega) = \frac{\int_{\mathrm{QW}} |E_z(\omega)|^2 dV}{\int_{\mathrm{QW}} dV}. \quad (1)$$

The distribution of the E_z component is computed by using a commercial software (COMSOL) [40]. The 2D computational domain is composed of an air layer, an Au grating layer (0.5 μm thick, period of 15 μm, and 50% duty cycle), a 0.4 μm thick upper contact layer, a 4.14 μm thick MQW layer, a 0.8 μm thick bottom contact layer, and a 650 μm thick substrate. A perfect match layer is set to absorb the reflected field energy from the grating-device surface. At the termination of the substrate, the perfect electric conductor boundary

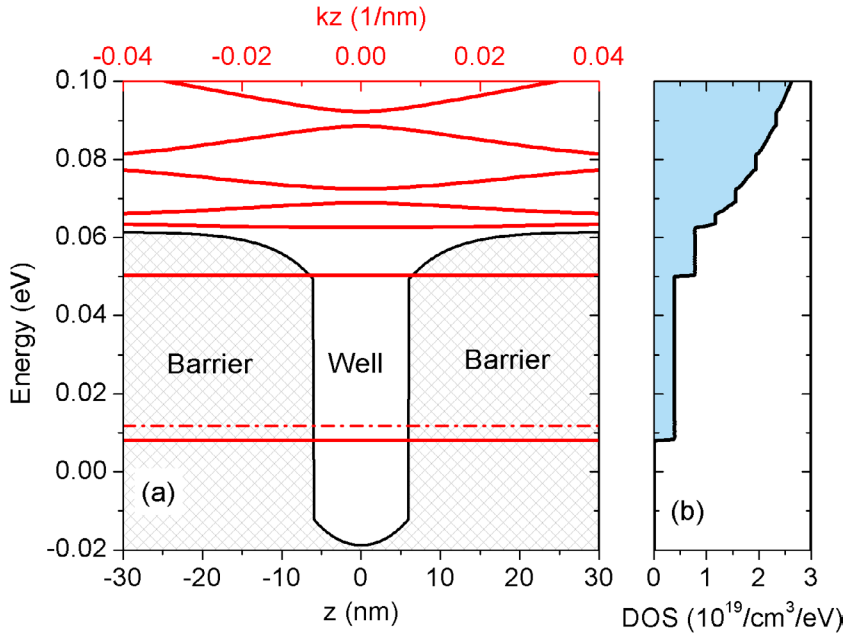

Figure 1. (a) Band structure, solid lines: subbands, dash-dot line: Fermi energy, and (b) density of states (DOS). The designed peak response frequency is about 9.9 THz (energy difference between the first excited subband and the ground subband).

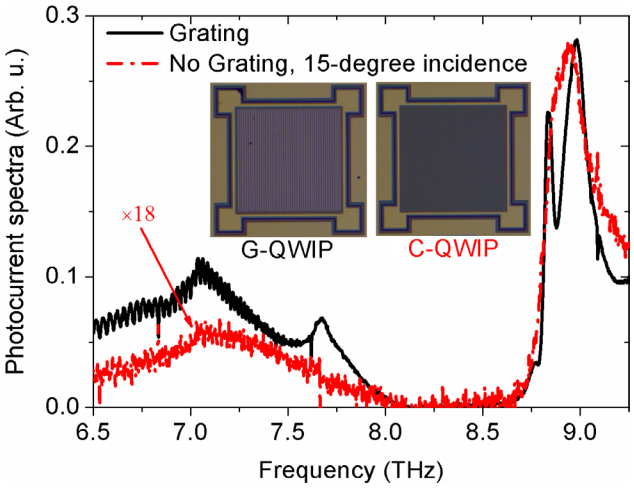

Figure 2. Photocurrent spectra (0.1 cm^{-1} frequency resolution) of the terahertz C-QWIP under 15° oblique illumination and the terahertz G-QWIP under illumination of normal incidence beam at temperature of 5.0 K and at bias of 0.6 V. Insertion: optical micrographs of G-QWIP and C-QWIP. The devices are in vacuum for the above measurements.

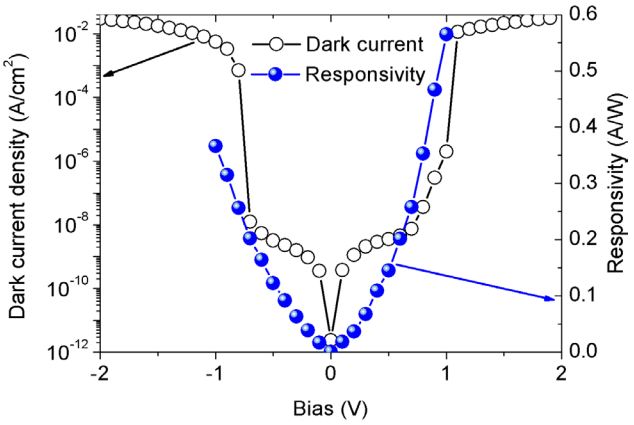

Figure 3. Dark current-density-voltage curve in voltage sweeping mode and peak responsivity (8.98 THz) with respect to the bias voltage of the terahertz G-QWIP. The device is operated at 5.0 K.

condition is set to mimic the metal mount holder. The Floquet periodic condition is applied in the x direction. A terahertz plane wave propagates along the z direction. Because the Al mole concentration of the AlGaAs barrier and the averaged Si doping concentration in the MQW layer are both very low, the MQW layer is replaced by a homogenous intrinsic GaAs layer to reduce the number of finite elements. The permittivity of doped GaAs is given as [35],

$$\varepsilon(\omega) = \frac{\omega_{\mathrm{TO}}^2(\varepsilon_s-\varepsilon_\infty)}{\omega_{\mathrm{TO}}^2-\omega^2-j\omega\Gamma_{\mathrm{TO}}} + \epsilon_\infty\left[1-\frac{\omega_{pi}^2}{\omega(\omega+j\Gamma_p)}\right], \quad (2)$$

where ω_{TO} is the circular frequency of transverse optical (TO) phonon in GaAs, $\varepsilon_s = 12.85$ and $\varepsilon_\infty = 10.88$ are the static- and high-frequency relative permittivities of GaAs, respectively, j is the unit of imaginary, and Γ_{TO} and Γ_p are the damping constants of TO phonon and electron plasmon, respectively. $\omega_{pi} = \sqrt{n_i e^2/(\varepsilon_0\varepsilon_\infty m^*)}$ is the angular frequency of electron plasmon in the upper contact layer ($i = 1$), the MQW layer ($i = 2$), and the bottom contact layer ($i = 3$), where n_i is the doping concentration ($n_1 = n_3 = 2.0 \times 10^{17}$ cm^{-3}, $n_2 = 0$), e is the electron charge, ε_0 is the vacuum permittivity, and $m^* = 0.067m_0$ is the effective mass of electrons in GaAs with m_0 being the electron mass. The relative permittivity of gold is calculated by using the Drude model with $\omega_{p,\mathrm{Au}} = 1.11 \times 10^{16}$ Hz and $\Gamma_{p,\mathrm{Au}} = 8.33 \times 10^{13}$ Hz [22]. In our calculations, ω_{TO} and Γ_{TO} are free parameters to be estimated by fitting the computational results to experimental data.

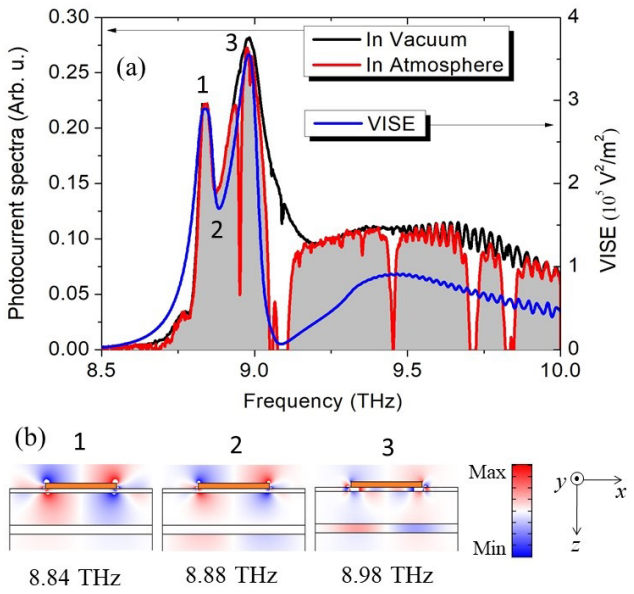

Figure 4. (a) Experimental photocurrent spectra measured in vacuum and in atmosphere of the terahertz G-QWIP and the computational VISE spectrum in the MQW regime; (b) electric field distributions of E_z component in the MQW region at frequencies of 8.84 THz, 8.88 THz, and 8.98 THz.

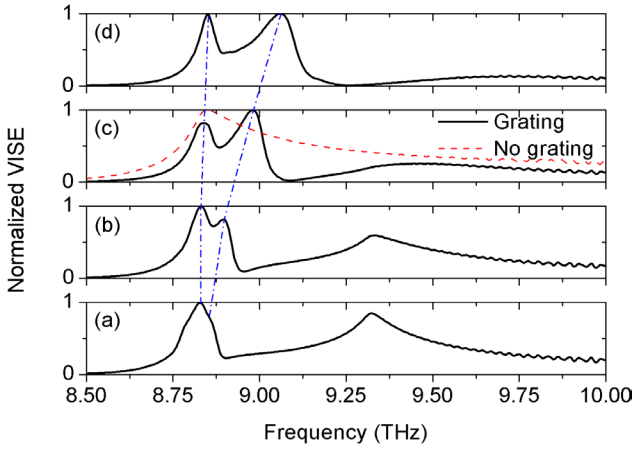

Figure 5. Computational γ spectrum (VISE) for different doping concentrations of the upper and bottom contact layers, (a) 0.5×10^{17} cm^{-3}, (b) 1.0×10^{17} cm^{-3}, (c) 2.0×10^{17} cm^{-3}, and (d) 3.0×10^{17} cm^{-3}.

Figure 4 shows the photocurrent spectra of the G-QWIP with the setup in vacuum (black line) and in atmosphere (red line) at a temperature of 5.0 K and at a bias of 0.6 V, the γ-value with respect to frequency, and E_z field distributions at frequencies of 8.84 THz, 8.88 THz, and 8.98 THz. There are many dips in the photocurrent spectrum introduced by water vapor absorption when the beam path is exposed to atmosphere. The dips related to water vapor absorption disappear and the influence of water vapor absorption is absent when the chamber of the Fourier spectrometer is in vacuum.

As shown in figure 4(a), the dominant two-peak feature positioned in the narrow frequency range of 8.80–9.00 THz in the photocurrent spectrum is well reproduced by the numerical result of the γ spectrum with the best fitting parameters $\omega_{\mathrm{TO}} = 8.13$ THz and $\Gamma_{\mathrm{TO}} = 0.25$ THz, which indicates that these features are determined by the field intensity in the MQW region, but not the inter-subband transition strength. From the small estimated value of Γ_{TO}, the dephasing time of TO phonon is $\tau_{\mathrm{TO}} = \frac{2\pi}{\Gamma_{\mathrm{TO}}} = 25.12$ ps, which is much longer than that of electron plasmon. For the C-QWIP, there exists only one-peak feature at about the LO phonon frequency on the γ spectrum, which is in agreement with the experimental photocurrent data (figure 2). We conclude that the two peaks (8.84 THz and 8.98 THz) correspond to two SPHP modes $\omega_{\mathrm{SPHP},1}$ $(\beta = 2\pi/p)$ and $\omega_{\mathrm{SPHP},2}$ $(\beta = 4\pi/p)$ with β the wave-vector of SPHP and p the grating periodicity. To further verify this conclusion, the dispersion relation of SPHP $\omega_{\mathrm{SPHP}}(\beta)$ should be investigated in detail [29, 32–34]. However, due to the multiple compositions (metal strips, doped contact layer, and intrinsic GaAs layer), we cannot derive an analytical expression of the dispersion relation of SPHP. There is an obvious discrepancy between the γ spectrum and the photocurrent spectrum in the frequency range of 9.0–10.0 THz. We attribute such a discrepancy to the energy-dependent scattering rate Γ_{TO} due to the relaxation of TO phonon to the other phonon modes. Figure 4(b) depicts the field distributions of E_z component at frequencies of 8.84 THz (peak), 8.88 THz (dip), and 8.98 THz (peak). It is interesting to note that the SPHP related field localizes beneath the metal strip of grating, but does not extend along the whole interface, which may originate from the difference of the dispersion relation of SPHP at the interfaces of gold-GaAs and air-GaAs. Moreover, the SPHP modes corresponding to the two peaks are $\omega_{\mathrm{SPHP},1}$ $(\beta = 2\pi/s)$ and $\omega_{\mathrm{SPHP},2}$ $(\beta = 4\pi/s)$, respectively, with s the width of metal strip.

As shown in figure 5, the doping concentration of contact layers has noticeable influences on the γ spectrum of the G-QWIP. For a small doping concentration of 0.5×10^{17} cm^{-3}, there is only a photoresponse peak, and the SPHP modes corresponding to different in-plane wave-vectors provided by the grating cannot be resolved. With the increase of doping concentration, two peaks due to SPHP modes of $\omega_{\mathrm{SPHP},1}$ $(\beta = 2\pi/s)$ and $\omega_{\mathrm{SPHP},2}$ $(\beta = 4\pi/s)$ appear, and the frequency difference between the two peaks increases with an increasing doping concentration. To clearly understand the complex behaviors of SPHP and increase the SPHP-related local field intensity, further investigations are needed.

4. Conclusion

In conclusion, a GaAs/AlGaAs terahertz QWIP with a peak response frequency of about 10.0 THz is designed, fabricated, and characterized. Two photocurrent response peaks at 8.84 THz and 8.98 THz are observed for the G-QWIP. The numerical VISE spectrum identifies that the two peaks are due to the field enhancement in the MQW region. Furthermore, there are no such two-peak features on the photocurrent spectrum for the C-QWIP (without grating coupler). Based on the above two facts, we attribute the two peaks to the SPHP-induced local field enhancement. By fitting the experimental data, the scattering rate of TO phonon $\Gamma_{\mathrm{TO}} = 0.25$ THz is

derived, which is much smaller than that of SPP. The small scatting rate of TO phonon indicates that the loss to SPHP is not as severe as that to SPP. Therefore, it is possible to obtain a high enhancement of local field intensity related to SPHP near an interface. We also find that the dispersion relation of SPHP is sensitive to the surrounding dielectric environment and doping concentrations of contact layers. Our results are useful to realize high performance SPHP-mediated terahertz photodetectors and other related terahertz devices.

Acknowledgments

We thank Professor Zhang Chao at University of Wollongong for revising our paper. Partial financial support was received from the Major Program of the National Natural Science Foundation of China (Grant No. 61731020), the National Key R&D Program of China (Grant Nos. 2016YFF0200306, 2017YFF0106304, and 2017YFF0106302), the National Natural Science Foundation of China (Grant Nos. 61775229, 61704181, 61575214, 61574155, and 61604161), and the Project of the Shanghai Science and Technology Committee (Grant Nos. 15DZ0500100, 15JC1403800, 15560722000, 15DZ0500103, and 17YF1429900).

ORCID iDs

XuGuang Guo https://orcid.org/0000-0003-1733-6478

References

[1] Lee Y S 2009 *Principles of Terahertz Science and Technology* (Berlin: Springer)
[2] Tonouchi M 2007 *Nat. Photon.* **1** 97–105
[3] Ferguson B and Zhang X-C 2002 *Nat. Mater.* **1** 26–33
[4] Rogalski A and Sizov F 2011 *Opto-Electron. Rev.* **19** 346–404
[5] Füser H and Bieler M 2014 *J. Infrared Millim. Terahertz. Waves* **35** 585–609
[6] Schneider H and Liu H C 2007 *Quantum Well Infrared Photodetectors: Physics and Applications* (Berlin: Springer)
[7] Ting D Z Y, Chang Y-C, Bandara S V and Gunapala S D 2007 *Appl. Phys. Lett.* **91** 073510
[8] Liu H C, Song C Y, SpringThorpe A J and Cao J C 2004 *Appl. Phys. Lett.* **84** 4068
[9] Luo H, Liu H C, Song C Y and Wasilewski Z R 2005 *Appl. Phys. Lett.* **86** 231103
[10] Guo X G, Cao J C, Zhang R, Tan Z Y and Liu H C 2013 *IEEE J. Sel. Top. Quantum Electron.* **19** 8500508
[11] Su X H, Yang J, Bhattacharya P, Ariyawansa G and Perera A G U 2006 *Appl. Phys. Lett.* **89** 031117
[12] Wu W, Bonakdar A and Mohseni H 2010 *Appl. Phys. Lett.* **96** 161107
[13] Palaferri D *et al* 2018 *Nature* **556** 85–8
[14] Gansch R, Kalchmair S, Genevet P, Zederbauer T, Detz H, Andrews A M, Schrenk W, Capasso F, Loncar M and Strasser G 2016 *Light Sci. Appl.* **5** e16147
[15] Kalchmair S *et al* 2012 *Opt. Express* **20** 5622
[16] Kalchmair S, Detz H, Cole G D, Andrews A M, Klang P, Nobile M, Gansch R, Ostermaier C, Schrenk W and Strasser G 2011 *Appl. Phys. Lett.* **98** 011105
[17] Guo X G, Zhang R, Cao J C and Liu H C 2012 *IEEE J. Quantum Electron.* **48** 728–33
[18] Guo X G, Zhang R, Cao J C and Liu H C 2012 *IEEE J. Quantum Electron.* **48** 1113–9
[19] Palaferri D, Todorov Y, Chen Y N, Madeo J, Vasanelli A, Li L H, Davies A G, Linfield E H and Sirtori C 2015 *Appl. Phys. Lett.* **106** 161102
[20] Paulillo B *et al* 2017 *Optica* **4** 1451–6
[21] Li H, Wan W J, Tan Z Y, Fu Z L, Wang H X, Zhou T, Li Z P, Wang C, Guo X G and Cao J C 2017 *Sci. Rep.* **7** 3452
[22] Zhang R, Guo X G, Cao J C and Liu H C 2011 *J. Appl. Phys.* **109** 073110
[23] Maier S A 2007 *Plasmonics: Fundamentals and Applications* (Berlin: Springer)
[24] Hillenbrand R, Taubner T and Keilmann F 2002 *Nature* **418** 159–62
[25] Novoselov K S, Mishchenko A, Carvalho A and Castro Neto A H 2016 *Science* **353** aac9439
[26] Basov D N, Fogler M M and de Abajo F J G 2016 *Science* **354** aag1992
[27] Le Gall J, Olivier M and Greffet J-J 1997 *Phys. Rev.* B **55** 10105–14
[28] Dai S *et al* 2014 *Science* **343** 1125–9
[29] Caldwell J D *et al* 2013 *Nano Lett.* **13** 3690–7
[30] Pozela J, Pozela K, Silenas A, Sirmulis E and Juciene V 2013 *Appl. Phys.* A **110** 153–6
[31] Feng K, Streyer W, Zhong Y, Hoffman A J and Wasserman D 2015 *Opt. Express* **23** A1418–33
[32] Streyer W, Law S, Rosenberg A, Roberts C, Podolskiy V A, Hoffman A J and Wasserman D 2014 *Appl. Phys. Lett.* **104** 131105
[33] Vassant S, Marquier F, Greffet J J, Pardo F and Pelouard J L 2010 *Appl. Phys. Lett.* **97** 161101
[34] Guo X G, Tan Z Y, Cao J C and Liu H C 2009 *Appl. Phys. Lett.* **94** 201101
[35] Klingshirn C 2005 *Semiconductor Optics* 2nd edn (Berlin: Springer)
[36] Gu L L, Guo X G, Fu Z L, Wan W J, Zhang R, Tan Z Y and Cao J C 2015 *Appl. Phys. Lett.* **106** 111107
[37] Gu L L, Zhang R, Tan Z Y, Wan W J, Yin R, Guo X G and Cao J C 2014 *J. Phys. D: Appl. Phys.* **47** 165101
[38] Liu H C, Buchanan M and Wasilewski Z R 1998 *Appl. Phys. Lett.* **72** 1682–864
[39] Guo X G, Gu L L, Dong M, Cao J C, Liu H C and Guo F M 2013 *J. Appl. Phys.* **113** 203109
[40] Multiphysics Modeling and Simulation Software COMSOL (www.comsol.com)